Case Studies in Thermal Engineering 39 (2022) 102457

Contents lists available at ScienceDirect

Case Studies in Thermal Engineering

journal homepage: www.elsevier.com/locate/csite

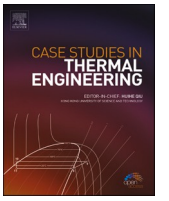

Slowly-closing valve behaviour during steam machine accelerated start-up

Mateusz Bryk [a,*], Mariusz Banaszkiewicz [a], Tomasz Kowalczyk [a], Waldemar Dudda [b], Paweł Ziółkowski [c]

[a] Energy Conversion Department, Institute of Fluid-Flow Machinery, Polish Academy of Sciences, Fiszera 14 st., 80-231 Gdańsk, Poland
[b] Faculty of Technical Sciences, University of Warmia and Mazury, Michała Oczapowskiego 2 Streeet, Olsztyn, Poland
[c] Faculty of Mechanical Engineering and Ship Technology, Gdańsk University of Technology, Narutowicza 11/12 st., 80-233, Gdańsk, Poland

ARTICLE INFO

Keywords:
Thermovision
Thermal-FSI analysis
Accelerated steam turbine start-up
Experiment validation
CFD/CSD calculations

ABSTRACT

The paper discusses the state of stress in a slowly-closing valve during accelerated start-up of a steam turbine. The valve is one of the first components affected by high temperature gradients and is a key element on which the power, efficiency and safety of the steam system depend. The authors calibrated the valve model based on experimental data and then performed extended Thermal-FSI analyses relative to experiment. The issue is important as determining the possibility of accelerating the start-up of a steam turbine while not exceeding the strength limit in the design of the steam valve. The shorter the startup time, the more environmental and economic benefits. The most important results of the work include the possibility to reduce the start-up time of a steam machine without excessive strain on the valve structural components and not to exceed the stress limits. The important news for the industry is that there is no need to change the valves construction in terms of accelerated start-up of the steam engine. The results of the work confirm the belief that fast start-up of a steam turbine is possible without large capital expenditures for design changes in the components of the steam system.

Nomenclature

c_n	– averaged steam flow velocity, m/s
C_p –	specific heat capacity, J/kgK
e	– total energy, J/m^3
E –	Young modulus, MPa
p	– pressure, N/m^2
$\dot{m}_n$	– steam flow, ($n = 1, 2, 3$), kg/s
r	parameter of isotropic hardening
S_e –	total energy source
S_k	– k source, kg/m^{3}s
S_n	– flow area of the valve, m^2
S_r –	isotropic hardening source

* Corresponding author.
E-mail address: mbryk@imp.gda.pl (M. Bryk).

https://doi.org/10.1016/j.csite.2022.102457
Received 7 March 2022; Received in revised form 17 September 2022; Accepted 28 September 2022
Available online 4 October 2022

S_ε – ε sources, kg/m^{4}s
T – temperature, K or °C
t – time, s
v – specific volume, m^3/kg

Notation for vector quantities
$\boldsymbol{\alpha}$ – beck-stress tensor of kinematical hardening
$\mathbf{v}$ – velocity vector, m/s
$\mathbf{b}$ – mass force vector, m/s^2
$\mathbf{e}_i$ – unit direction vector
$\boldsymbol{\varepsilon}^{pl}$ – plastic deformation tensor
$\mathbf{I}$ – unit tensor
$\mathbf{J}_k$ – diffusive flux of k, kg/m^{2}s
$\mathbf{J}_\varepsilon$ – diffusive flux of ε, kg/m^{2}s
$\mathbf{J}_r$ – kinematic flux of isotropic hardening
$\boldsymbol{\sigma}$ – solid stress tensor, N/m^2
$\boldsymbol{\tau}^c$ – total stress tensor of irreversible phenomena
$\boldsymbol{\tau}$ – molecular stress tensor
$\mathbf{R}$ – turbulent stress tensor
$\mathbf{S}_{pl}$ – plasticity source
$\mathbf{S}_\alpha$ – kinematical hardening source
$\mathbf{D}$ – diffusive stress tensor
$\mathbf{q}^c$ – total heat flux, W/m^2
$\mathbf{q}$ – molecular heat flux
$\mathbf{q}^t$ – turbulent heat flux
$\mathbf{q}^{ph}$ – phase change heat flux

Greek symbols
$\alpha = S_{min}/S_{max}$ – geometry fraction of a flow canal
β – coefficient of thermal expansion, 1/K
δ_{ij} – Kronecker's delta
λ – thermal conductivity, W/mK
ν – Poisson's ratio
ρ – density, kg/m^3
σ – reduced stress (scalar), MPa
Φ – strain energy density, J/m^3

Subscripts
m – model
p – prototype
$n = 1, 2, 3, 4$ –main planes of a valve
red – reduced stress
HMH – Huber-Mises-Hencky
r, θ, z – main cylindrical directions of the stress tensor

Acronyms
CFD – Computational Fluid Dynamic
CSD – Computational Solid Dynamic
FSI – Fluid Solid Interaction
FVM – Finite Volume Method
RES – Renewable Energy Sources
HMH – Huber-Mises-Hencky
WAT – Wojskowa Akademia Techniczna (Military University of Technology)
SOFC – solid oxide fuel cells

SOEC – solid oxide electrolyse cells.

1. Introduction

Every start-up of a steam machines is a complex technical and operational issue. When starting from a cold (environment) state, the temperature of metal elements increases in a few minutes by several hundred degrees. This is accompanied with thermal expansion of

the metal and thermally induced displacements. Thus, deformations of metal elements are observed as well as an increase in stress in the metal especially when backlashes between elements are too small. These phenomena occur at a different rate for hull elements and for the rotor [1]. Other elongations of rotor and hull elements lead to reduction of technological backlash and increase the risk of blurring the turbine components [2]. Frequent load changes and high heating speeds of metal parts lead to rapid thermal fatigue and material cracking. Thermal deformations can lead to permanent deformation of different metal as well as composite elements [3,4].

Our analysis is dedicated to quite novel applicability of valves [4]. Recently, steam valves are used for large-scale technologies called "power to fuel", that are based on the extensive and accelerated expansion of wind and solar energy. In particular, high temperature (800-1000 ^{o}C), high pressure (up to 20 MPa) solid oxide electrolysis cells (SOEC) have been widely applied as an effective, environmentally friendly, economically attractive and very innovative robust technologies for conversion of electrical energy into hydrogen [5,6].

From our study of environmental data [7] it become obvious that wind and solar energy sources are very unpredictable in their power and frequency of usability. This fact turns our attention that due to the constantly growing share of renewable energy in the Polish power system, conventional units are forced to change the nature of their work in such manner that it must be similar with the nature of work of renewable sources.

It is known that the inertia of conventional sources is much greater than that of renewable sources. This results in extra-designed changes in the power output of the power units, for which they were not designed. The result of such quick electrical power output changes is, generally speaking, accelerated damage of metal elements which leads to uncontrolled failure [8,9].

Concepts of effective cooperation of renewable sources with conventional sources are currently being developed in Poland. In short, the following solutions can be used to increase the flexibility of steam blocks:

- energy stores:
  - compressed or liquid air storages [10].
  - heat stores in the steam circuit [11].
  - storage of hydrogen and hydrogen based synthetic fuels [12].
  - thermal energy storage [13].
- advanced temperature control of the most stressed machine elements [14].
- improving the efficiency of the steam cycles [15,16].
- advanced modeling to determine non-design constraints using elastic-plastic material adaptation [17].

The previous work by the authors [18] demonstrated the possibility of reducing the start-up time of the turbine itself from the warm state by 1 h using steam cooling. This procedure reduces the stress in the turbine structure during accelerated start-up. Going further in this direction, the aim of this work is to determine the possibility of carrying out accelerated start-up of a steam machine from the side of slowly-closing valves. Earlier works state the possibility of safe operation of the considered accelerated start-up solution by means of cooling steam injection [19]. In addition, Siemens proposed the use of steam injection with lower parameters for cooling turbine components exposed to high temperature values [20,21]. Additionally, promising results for ultra-fast start-up is presented by Kraszewski B [22].

The important basic elements of the steam machines are valves. The valve is one of the first components to be affected by high temperature gradients. The reliability of the valve is essential for the safe operation of the steam machine. The valve must maintain its operability despite the thermal stresses acting on it [23]. Thus, having previously identified the possibility of accelerating the start-up of a steam machine, the authors focus on the effect of this process on the valve. Since valve failures occur due to thermal loads [24,25], the effect of accelerated startup on valve behavior should be investigated.

The analysis also showed that the live steam tee, despite its massive walls, is not an element limiting the start-up time of a steam device. A similar line of reasoning was adopted to valves by Li et al. [26] and Jalali et al. [3].

Li has defined that the conjugate heat transfer simulation using the SST model could accurately determine spatiotemporal variation of thermal behaviors of the turbine valve in a short transient period of its fast start-up process, however, the calculations carried out relate only to the thermal condition of the device, no strength analyses were carried out.

Jalali has carried out failure analysis in a steam turbine stop valve without performing flow calculations. The set temperatures were in the transient thermal module of the Ansys Mechanical program, and based on them he determined that the expansion and contraction movements of the turbine were the main cause of fatigue and crack in the stop valve body.

So far, the effect of both start-up (which is not a simple issue) and accelerated start-up on valve operation has not been investigated.

In the literature the effect of an off-design thermal load change on the stress state of the valve has not been described. In the literature one can find works treating:

- influence of opening and closing process and its influence on external performance and internal flow characteristics [27];
- performance, flow patterns and cavitation phenomena of ball valve [28];
- dynamic characteristics of valve, but only fluid forces and pressures are investigated [29];
- determination of valve erosion based on CFD calculations [30];
- Thermal shock during the opening of the safety valve where the 3D thermo-mechanical coupling simulation has been conducted without CFD calculations [31];
- Flow rate analysis of valve, where only pressure and velocity was taken into consideration [32];
- Fatigue life prediction of regulating valves without CFD analysis [25];
- Computational fluid dynamics of steam flow in a turbine control valve without strength analysis [33];

Additionally, we can find works on rapid valve opening [34] and thermohydraulic effects of safety relief valves [35].

The effect of design acceleration and off-design acceleration on thermal stress in a steam valve has not been addressed as a comprehensive Thermal-FSI analysis.

In this paper, the authors calibrated the valve model based on Professor Orloś experiment [36]. Then, having the numerically mapped model, the authors extended the analysis of the valve made in the experiment with the phenomena occurring during the accelerated start-up.

Validation of the model first involves the numerical generation of the geometry and the use of the equations governing the physical model. Then, after obtaining the numerical results of the calculations, one proceeds to compare the experiment with possible corrections to obtain a satisfactory agreement.

The work represents a search for answers to the questions:

- whether fast start-up of a steam engine is possible and safe for the design of a steam valve,
- what temperature gradients affect the valve in the transient state,
- whether the state of stress in the valve structure is safe.

2. Analyzed geometry of the experimental valve

In order to perform the analysis, the authors used an experiment conducted at WAT (Military University of Technology at Warsaw) by Orłoś et al. [36]. The analysis of temperature distribution and on its basis the distribution of stresses in the quick-closing valve was performed. The geometry of the valve is shown in Fig. 1, where characteristic dimensions are shown.

The actual model is made of E-2 epoxy resin hot cast in sheet metal moulds. The castings have been machined. The machined parts were armed with sensors and then glued together with epoxy resin E-5. Based on the available documentation, a three-dimensional geometry of the valve was made. For the sake of simplicity, the screw connection was not reproduced in the model.

3. The experiment description

The experiment has consisted of the following stages: making a model valve made of epoxy plastic; application of the thermovision apparatus for testing stationary and non-stationary temperature fields on the valve surface; post-determination of mass-rates, steam velocities and heat transfer coefficients; determination of the thermal stresses by means of reconstructed field of temperature. The domain contains 98 sensors (Fig. 1). More information can be found in Ref. [36].

Through the chamber was flowing hot air with the constant inlet condition $T_{in} = 74\ ^{o}\mathrm{C}$, $c_{in} = 60$ m/s.

4. Comparative analysis

The authors have reproduced the WAT (Military University of Technology) experiment numerically in order to validate the numerical model with a real valve model. Comparison of the experimental results of temperature field distributions and then stress fields was used as a reference for the reliability of subsequent accelerated start-up analyses on the valve side.

In addition, the numerical analysis is also an additional verification of the WAT-experiment. The authors will determine the accuracy of the similarity theory of thermo-elastic resemblance used in the WAT-experiment.

4.1. Model CFD

For the fluid flow simulation, three basic formulas of conservation must be fulfilled. These three main formulation which describe CFD are presented below [18,37]:

Conservation of mass equation:

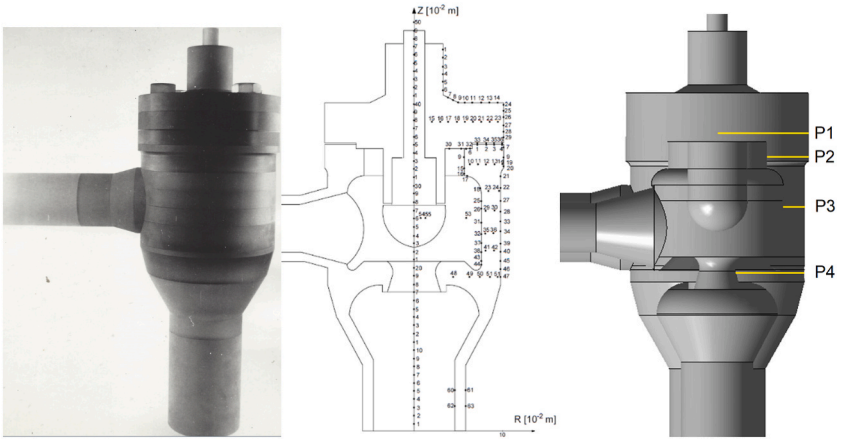

Fig. 1. View on geometry of the analyzed valve, axial section of the valve with visible sensor armature and model with marked measuring planes $P1 - P4$.

$$\partial_t(\rho) + \mathrm{div}(\rho\mathbf{v}) = 0 \tag{1}$$

Conservation of momentum equation:

$$\partial_t(\rho\mathbf{v}) + \mathrm{div}(\rho\mathbf{v}\otimes\mathbf{v} + p\mathbf{I}) = \mathrm{div}(\boldsymbol{\tau}^c) + \rho\mathbf{b} \tag{2}$$

Conservation of energy equation:

$$\partial_t(\rho e) + \mathrm{div}\left[\left(e + \frac{P}{\rho}\right)\rho\mathbf{v}\right] = \mathrm{div}\left(\mathbf{q} + \mathbf{q}^t + \boldsymbol{\tau}^c\mathbf{v} + \mathbf{q}^D\right) + \rho\mathbf{b}\bullet\mathbf{v} \tag{3}$$

These are balance equations in the conservative form, where: ρ - gas density, [kg/m^3]; $\boldsymbol{\tau}^c = \boldsymbol{\tau} + \mathbf{R} + \mathbf{D}$ - total tensor of irreversible stress, [Pa] that consist molecular, turbulent and diffusive parts; $\mathbf{v} = v_i\mathbf{e}_i$ – mean velocity, [m/s]; $\mathbf{q}$ – molecular heat flux, [W/m^2]; $\mathbf{q}^t$- turbulent heat flux, [W/m^2]; $\mathbf{q}^D$- diffusive heat flux, [W/m^2]; p - pressure, [Pa]; $e = u + \frac{1}{2}\mathbf{v}\bullet\mathbf{v}$- specific total energy, [J/kg]; $\mathbf{b} = -9,81\mathbf{e}_z$ [m/s^2].

Additionally, above set of three governing equation, i.e. (1-3), were complemented by two evolution equations for parameters, which allow to define turbulent tensor $\mathbf{R}$ components [17]. The first is the evolution equation concerning turbulent energy k (4):

$$\partial_t(\rho k) + \mathrm{div}(\rho k\mathbf{v}) = \mathrm{div}(\mathbf{J}_k) + S_k \tag{4}$$

And the second one is the evolution equation concerning energy dissipation ε (5):

$$\partial_t(\rho\varepsilon) + \mathrm{div}(\rho\varepsilon\mathbf{v}) = \mathrm{div}(\mathbf{J}_\varepsilon) + S_\varepsilon \tag{5}$$

4.2. Model CSD

In order to a solve solid stated problem, basic equations used in CSD simulations and equation governing species transport are used [38]. Note that a common form of CFD and CSD is required since during a numerical simulations there are need for simultaneous calculations and numerous exchanging of fluid and solid resulting data. Therefore, speaking on CSD one must start from the following "conservation form" of CSD [18]:

$$\frac{\partial}{\partial t}\begin{Bmatrix}\rho\\ \rho\mathbf{v}\\ \rho e\\ \rho\mathbf{e}^{pl}\\ \rho\boldsymbol{\alpha}\\ \rho r\end{Bmatrix} + \mathrm{div}\begin{Bmatrix}\rho\mathbf{v}\\ \rho\mathbf{v}\bigotimes\mathbf{v}\\ \rho e\mathbf{v}\\ \rho\mathbf{e}^{pl}\bigotimes\mathbf{v}\\ \rho\boldsymbol{\alpha}\bigotimes\mathbf{v}\\ \rho r\mathbf{v}\end{Bmatrix} = \mathrm{div}\begin{Bmatrix}0\\ \boldsymbol{\sigma}\\ \boldsymbol{\sigma}\,\mathbf{v} + \mathbf{q}^c\\ 0\\ 0\\ \mathbf{J}_r\end{Bmatrix} + \begin{Bmatrix}0\\ \rho\mathbf{b}\\ \rho S_e\\ \rho\mathbf{S}_{pl}\\ \rho\mathbf{S}_\alpha\\ \rho S_r\end{Bmatrix} \tag{6}$$

where: $\rho = \rho(\boldsymbol{x},t)$- density depends, in general, on time t and location $\boldsymbol{x}$, $\mathbf{v} = \mathrm{v}_i\mathbf{e}_i$- velocity, $\mathbf{e}_i$ – unit direction vector, $\boldsymbol{\sigma} = \sigma_{ij}\mathbf{e}_i\bigotimes\mathbf{e}_j$- thermodynamic stress tensor,$\mathbf{I} = \delta_{ij}\mathbf{e}_i\otimes\mathbf{e}_j$- unit tensor, δ_{ij}- Kronecker's delta, $\mathbf{b}$ - mass force of gravity, $e = u + \frac{1}{2}\mathbf{v}^2$- sum of internal and kinetic energy, $\mathbf{q}^{\mathrm{c}} = \mathbf{q} + \mathbf{q}^{\mathrm{T}}$- total heat flux (which contains molecular heat flux and turbulent heat flux respectively). Next $\boldsymbol{\varepsilon}^{pl}$ is plastic deformation tensor, $\boldsymbol{\alpha}$ - is the beck-stress tensor of kinematical hardening, r - parameter of isotropic hardening, $\mathbf{J}_r$, - kinematic flux of isotropic hardening. Finally the set of governing equations are closed via the density sources: mass, momentum, energy: S_e , plasticity $\mathbf{S}_{pl}$, kinematical hardening $\mathbf{S}_\alpha$ and isotropic hardening S_r . In particular, calibration of these sources needed more detailed analysis based on dedicated experiments and have been done in the papers by Dudda at al [39–41].

4.3. Thermal-FSI tools

Thermal-FSI analysis consists in CFD analysis, the results of which are exported to a solid state solver (CSD). Next, the CSD solver on the basis of imported data (temperature, pressure) determines the stress and displacements in the analyzed geometry.

As we know, in the literature, there are two types of Thermal-FSI [29–31] analysis: *one way FSI* and *two way FSI*. We have a difference to the momentum-FSI where, in the one way FSI, after CFD calculations, the solution of pressure field is exported to the CSD solver and the stress and displacements determined on their basis. In *one way* thermal-FSI, the cooling or heating of fluid by solid body is realized with the Neumann type boundary conditions.

In the case of two-way Thermal-FSI analysis, both models (CFD and CSD) are coupled together during the entire simulation via energy equation balance. Precisely speaking this coupling takes place on a common surface between solid and fluid domain, where we are staying the crucial boundary condition (7) [18]:

$$\left(\mathbf{q} + \mathbf{q}^t + \mathbf{q}^{rad} + \mathbf{q}^D\right)\bullet\mathbf{n}_{|solid} + \left(\mathbf{q} + \mathbf{q}^t + \mathbf{q}^{ph}\right)\bullet\mathbf{n}_{|fluid} = 0 \tag{7}$$

The work involved two-way Thermal-FSI analyzes. Temperature fields were automatically imported, both, from solid to fluid and *vice versa* from fluid to solid. Finally, from the field of temperature, a new pressure in fluid and new thermal stress fields in solid, in the analyzed numerical domain were determined.

4.4. FVM discretisation of the simulation domain

The valve 3D geometry was discretized using the finite volume method (FVM). Both the liquid and solid were discredited using triangular volumes. A wall layer was used. The calculation domain consists of 4 million elements for the fluid and 4.5 million for the

solid.

The mesh independence was verified by comparing the temperature at path P4. The reason that the average temperature at the path is selected for mesh independence check is that its value affects the allowable stress when evaluating the stress of the valve. Meanwhile, the path is selected due to its thin wall thickness and large temperature gradient along the path. Four different meshes with numbers [417,817 (coarse), 1,100,192 (medium), 4,763,254 (upper medium) and 15,129,768 (fine)] are generated. Table 1 shows the transient mean temperature at selected locations calculated with different grids. It shows that the maximum difference of temperature for Grid 1 is 3.20 °C, for Grid 2 is 1.81 °C, for Grid3 is 1.80°C, and for Grid4 0.87°C.

Taking into consideration the calculation time and relatively small differences between the temperature values, Grid3 can be regarded as a mesh independent solution. The fluid domain contains 3,125,487 elements. The solid domain contains 1,637,767 elements. More information about FVM can be found in the literature [31]. Table 1 represents the results of the temperature in the analyzed path for 4 types of grids.

4.5. Boundary and initial conditions

In the experiment the valve was heated by air at atmospheric pressure from the laboratory temperature $T_0 = 288^oK$ up to the temperature of hot air equal to $T_{air} = const = 356^oK$. In fluid CFD analysis was used a real gas model. It means, that the inlet data was set at a constant speed and temperature: $c = 60$ m/s and 356^oK by 1 h. Not only the inlet set parameters were constant in time but on the external wall of the valve a condition of natural convection was set at constant ambient temperature of: 288^oK.

4.6. Field of temperature - results

Even if we are focused on an analysis of the rate of solid heating, one must check to follow conditions within the CFD domain. Especially, it is important to inform about the flow velocities and a condition for flow trotting by appearing a mass flux blockades due to shock surface. A such an internal flow structure changes the conditions for surface heat transport. Since we have constant inlet velocity $c = 60$ of m/s during the experiment, it means that the heat exchange conditions are advantageously distributed in the whole internal surface.

Even if one has a constant inflow of hot air during the whole experiment, the solid temperatures are still growing. This sub-section presents the distribution of temperature fields on the valve surface and in characteristic planes of the analyzed geometry. The results obtained were compared with the experiment. A comparison of temperature distributions is shown in Fig. 2–4.

It follows that, the Thermal-FSI calculations are well aligned with the thermal imaging performed in the experiment. The highest temperature values are observed on the outer surface of the intake channel. After 1 h, the temperature is redistributed and the established heat exchange is reached.

Fig. 5 presents temperature values in individual valve sections. One can find, that after 1 h, simulated temperatures values in four sections P1, P2, P3 and P4 are in an appropriate agreement with the epoxy-WAT experiment.

4.7. Thermal stress distribution

In CSD simulation we have assumed that the material properties of epoxy material are constant (not dependent from the temperature). However, the data of the change of steel properties $(E, \nu, \lambda, \alpha, c_p)$ with grooving temperature were taken from the experiment by Dudda [40,41,42]. Appropriate UDF dates were implemented in papers by Badur and Bryk [17,18].

The results were compared the main stresses: σ_b – bending stress, σ_s - shear stress, σ_t - tensile stress. Note, that stress values were obtained after 1 h measurements (nearly-stationary case). Date for the WAT-epoxy experiment (epoxy and metal) were compared with stress values determined by our CSD method.

Three stress values in P1 cross-section in the hot state of the epoxy valve can be analyzed in Fig. 6.

Fig. 6 shows a comparison of the radial, vertical and circumferential stress values in P1 section. The results of the stress results from the experiment are described in Section 3. The stress courses determined by WAT-epoxy and CSD are similar in character.

It follows, that axially-symmetric WAT-epoxy model in comparison with full 3D model can leads to quite correct results. In the case of a real object (a metal valve), an attempt was made to introduce external ties in the form of equal radial displacements of nodes at the interface between the valve chamber flange and cover.

Fig. 7 shows the stress distribution for the steel model, analogously to the graph in Fig. 6. As with the Epoxy model, the stress values obtained for the steel model are similar. The differences between WAT-steel and CSD are shown in the terms of stress values.

4.8. Comparative analysis - summary

Differences in stress values result from the accepted calculation model. The results of the CSD analysis seems to be more reliable

Table 1
Temperature values in path P3 for 4 grid types.

x[m]	Experiment T[°C]	Grid1 T[°C]	Grid2 T[°C]	Grid3 T[°C]	Grid4 T[°C]
0.043	81.60	81.10	81.20	81.52	81.55
0.062	78.00	74.80	76.19	78.00	78.50
0.075	70.20	68.15	68.95	70.15	70.61
0.087	60.00	58.20	59.37	60.08	60.53
0.097	51.60	50.08	50.30	53.40	52.47
0.102	46.80	45.25	45.91	47.80	47.60

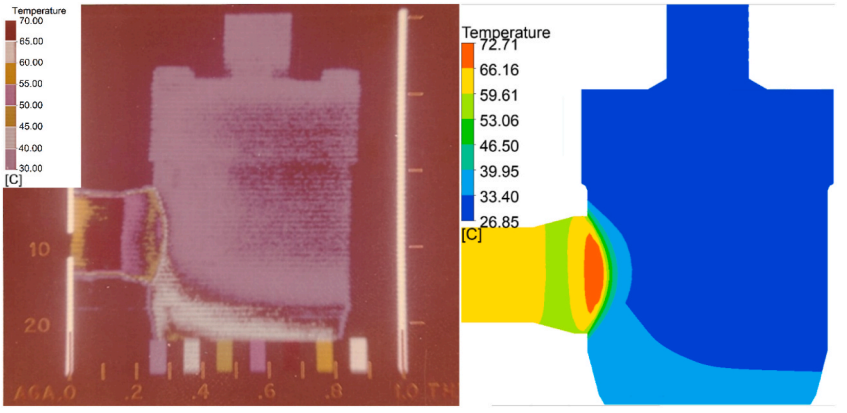

Fig. 2. Temperature distribution - 3 min after start up. Left - experiment, right – Thermal-FSI.

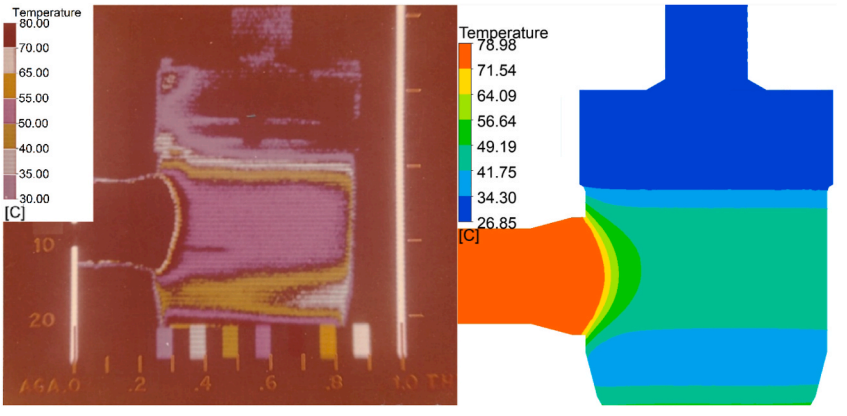

Fig. 3. Temperature distribution - 20 min after start up. Left - experiment, right – Thermal-FSI.

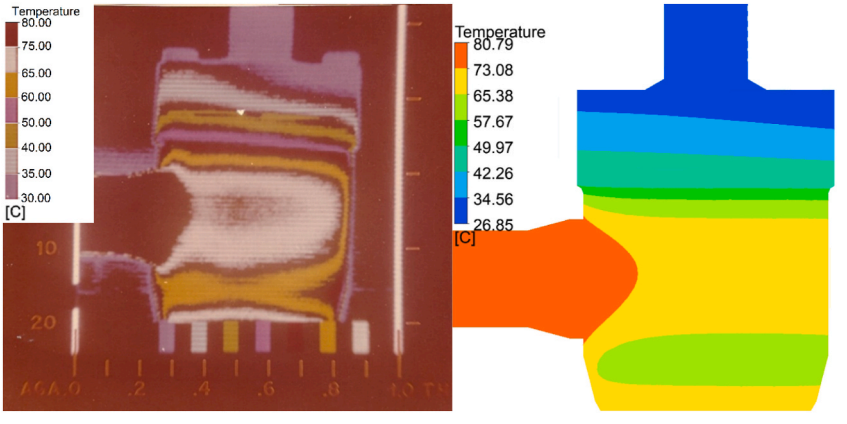

Fig. 4. Temperature distribution - 60 min after start up. Left - experiment, right – Thermal-FSI.

since the CSD model takes into account the exact temperature field, full 3D geometry, dependence of physical properties form the temperature and so on. Calculations made by the WAT-epoxy method [36] due to the year of their execution are considered to be correct, but more reliable are those made by the authors of the article.

Despite the differences in stress values determined by the CSD method, both methods return similar runs. For this reason, it was considered that the analyses made enable the use of the created CSD model for the analysis of quick valve start-up.

It means that both CFD and CSD models [43,44] are correctly calibrated and well suited for temperature measurements in the real model. Continuous, experimental temperature distributions have been obtained on the outer contour as well as in individual sections.

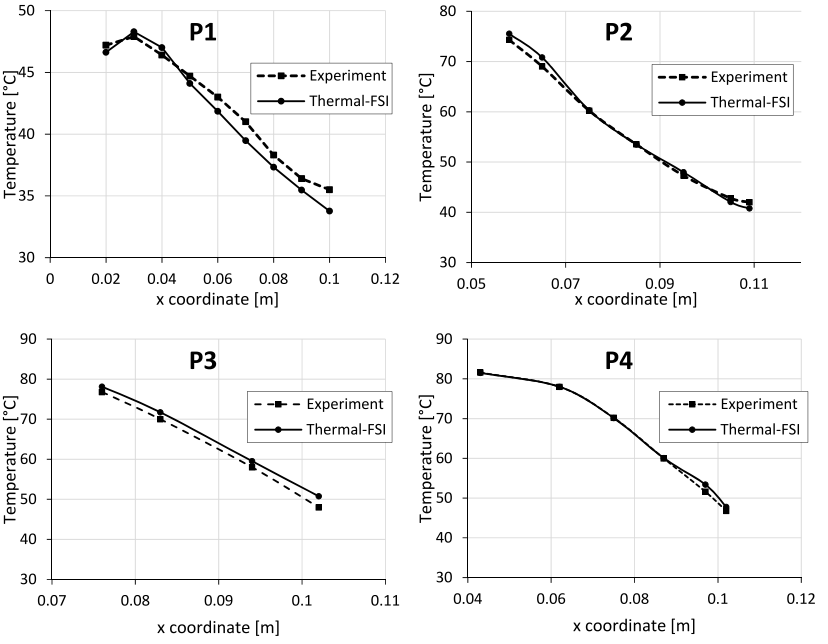

Fig. 5. Temperature distribution in section P1, P2, P3 and P4, after 1 h..

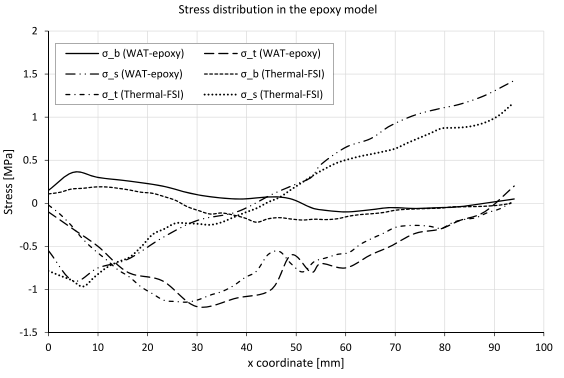

Fig. 6. Stress curves, after 1 h, at P1 cross-section. Comparison WAT-epoxy date with CSD calculations. Indexes: σ_b – bending stress, σ_s - shear stress, σ_t - tensile stress.

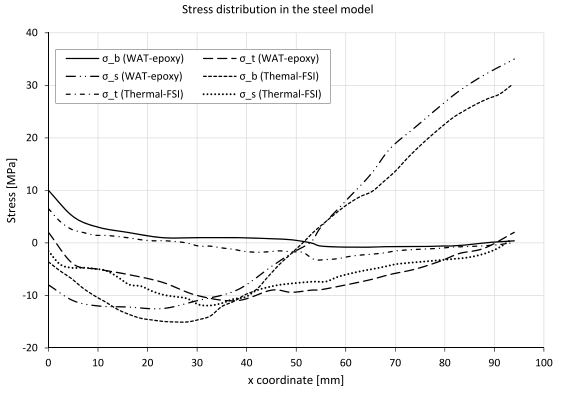

Fig. 7. Stress curves after 1 h at P1 cross-section. Comparison WAT-steel data with CSD simulations. Indexes: σ_b – bending stress, σ_s - shear stress, σ_t - tensile stress.

The results obtained in the adopted test method are characterized by high accuracy and readability. Let us note, that the temperatures along the contour of the WAT-epoxy model were assigned by Orłoś et al. [36] to the edge nodes as the boundary conditions for their axial-symmetric MES model. The highest temperature values are observed in the section P4.

5. 3D analysis of a full-scaled valve model

In comparison with the previous WAT-epoxy experiment, now the valve was re-modelled in such a manner that its geometry was scaled four times to match the size of the actual valve. The purpose of the analysis will be to check the valve behaviour under accelerated steam machine start-up conditions. It is important since, in the literature, there are data about different exploitation damage of valves (e.g., Duda and Rząsa [45,46])

5.1. Initial and boundary conditions

Steam tables are used for CFD modelling. The boundary conditions for flow are pressure and temperature as at the turbine inlet during start-up 3h and 2h. At the outlet of the domain, pressure and temperature parameters were set based on stationary calculations. On the external wall of the valve the condition of natural convection at the ambient temperature of 388^{o}K is set. Tables 2 and 3 show the parameters of live steam during 3h and 2h start-up.

6. Simulation results and discussion

6.1. Temperature change during 3h start-up

Fig. 8 shows the temperature redistribution of sections P1 to P4 at 3min 5min 10min 60min 120min and 180min.

The lowest temperature values are adopted by section P1, this is due to the thickness of the material in this plane and the fact that the analyzed plane is above the contact plane with the hot medium. The temperature gradient on the outer and inner wall takes the value of about 22^{o}K for the final start-up time.

The P3 plane is characterized by a temperature gradient value of 40^{o}K.

P4 has the highest temperature gradient. This is due to the direct contact of the hot medium with the metal and the element thickness in this plane. The temperature difference between the inner and outer wall here is about 100 K for the final run-up time.

6.2. Temperature change during 2h start-up

Fig. 9 shows the temperature redistribution in sections P1 to P4 during 3min 5min 10min 35min 70min and 120min.

The lowest temperature values, analogous to the 3h start-up, are in section P1. This is due to the thickness of the material in this plane and the fact that the analyzed plane is above the contact plane with the hot medium. The temperature gradient on the outer and inner wall takes on a value of about 25^{o}K for the final start-up time.

The temperature of the inner wall takes on a value at a similar level to that of the 3h start-up at 2h.

The P3 plane has a temperature gradient value of 55^{o}K.

The P4 plane has the highest temperature gradient value. This is due to the direct contact of the hot medium with the metal and the element thickness in this plane. The temperature difference between the inner and outer wall here is about 200^{o}K for the final run-up time.

Comparing the 3h and 2h start-up, it can be seen that the values of the temperature gradients between the outer and inner wall increase. This is most evident on the P4 plane, where the temperature gradient for the 2h start-up is 2 times higher than for the 3h start-up.

Higher temperature gradients will result in higher thermal stress values.

6.3. Stress behavior during start-up

On the basis of the obtained temperature field distributions, the stresses occurring in the valve were determined. The results are shown in the diagram in Fig. 10.

The stress waveform for the 3h start-up is standard for this type of case. After reaching the temperature value and adequate annealing of the geometry, the stresses decrease their value. The maximum stress value is 420 MPa.

In the case of a 2h start-up, higher temperature gradients are present in the geometry, which have an influence on the thermal stress. In this case the geometry is heated to a lesser extent than for the 3h start-up, which results in the fact that the stress value at 2h does not decrease compared to the earlier time as it does for the 3h start-up. The highest stress value is 468 MPa.

At the final stage of start-up, the stress takes the value of 391 MPa for 3h start-up and 468 MPa for 2h start-up.

Looking at the results of the analyses, the hypothesis that was made about the possibility of reducing the start-up time was verified

Table 2
Live steam pressure and temperature as a function of time during 3h start-up.

t (s)	T(^{o}K)	P (MPa)
0	573	1
1000	593	1
1600	658	5,2
7200	833	17,2

Table 3
Live steam pressure and temperature as a function of time during 2h start-up.

t (s)	T(°K)	P (MPa)
0	573	1
1500	593	1
2400	658	5,2
10800	833	17,2

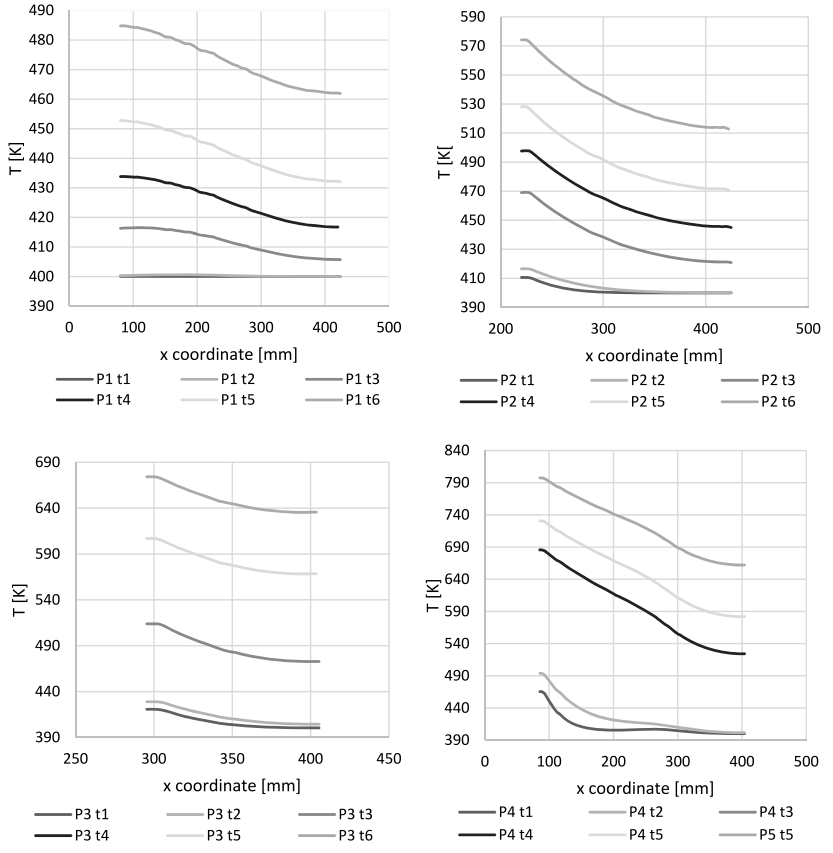

Fig. 8. Temperature distribution in section P1, P2, P3 and P4 during 3h start-up.

positively. The models used reliably reflect reality, which was confirmed by calibrating the model with experiment. So far, the literature has not dealt with off-design thermal loading of a steam valve, which was a challenge for the authors. The analyses were carried out as part of a broader issue related to the rapid start-up of a steam turbine. There are many papers in the literature where steam valve failures are analyzed as a result of operation that deviates from the design target.

The advantage of the Thermal-FSI tool over other simulation methods was used. The simulations performed return reliable results, with which the stress states in the valve can be estimated.

It is important to mention the limitations that come with the lack of an experiment for a full-scale real valve. The best research method would be analysis on a real model and then comparing it with calculations, but because of the hypothesis testing for the feasibility of the proposed changes, Thermal-FSI calculations are the best solution. We are talking about not having to build a test rig and take measurements.

An additional aspect is the lack of analyses for other components of the steam system that are exposed to increased heat loads (including steam supply pipelines). In order to be absolutely sure about the absence of negative impacts of heat loads on the steam system, additional elements (e.g., the aforementioned pipelines) would also need to be considered, as well as fatigue analyses. Such analyses as well as an experiment are planned for the future.

7. Conclusions

The paper presents the results of numerical modelling in terms of stress distribution in the components of the slow-closing valve for the design start-up (3h) and accelerated (2h) steam turbine. The model was validated on the example of the WAT-experiment using a

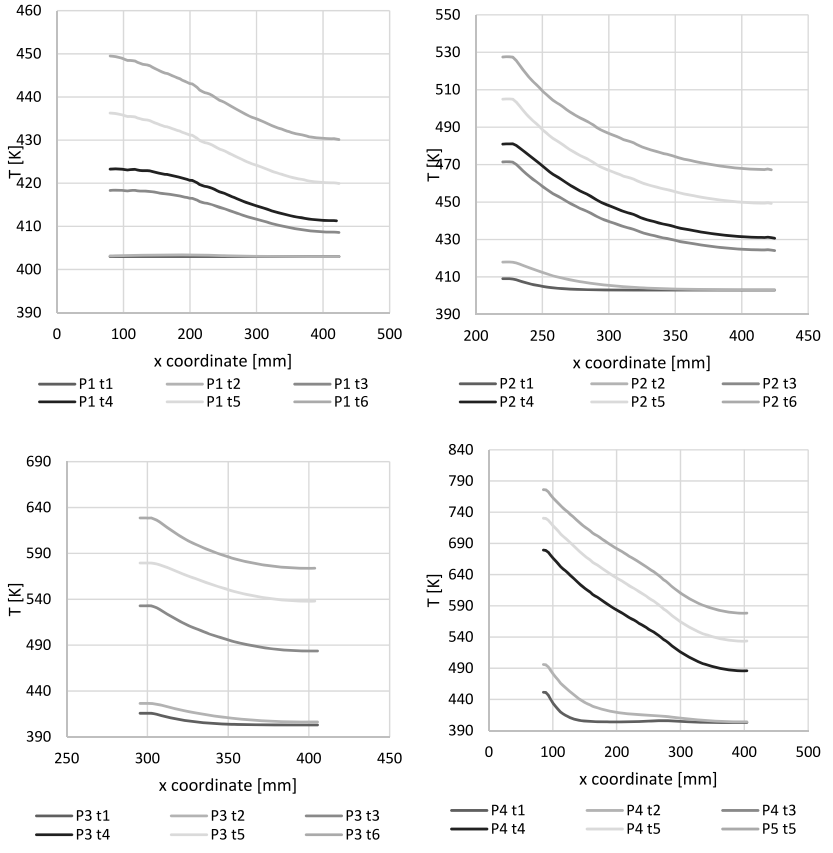

Fig. 9. Temperature distribution in section P1, P2, P3 and P4 during 2h start-up.

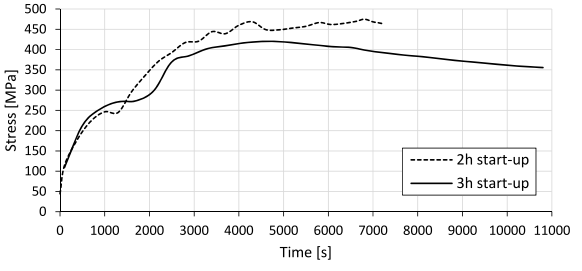

Fig. 10. Comparison of HMH-equivalent stress curves during 2h and 3h start-up.

valve made of epoxy resin in 1:4 scale. After validation of the model, a full-size valve made of ST12t steel was subjected to numerical analysis. In the case of project start-up, the maximum stress (HMH) occurs after 4500s and is 420 MPa.

We have the following conclusions:

- in the case of accelerated start-up, these stresses reach local peaks of 469 MPa, 467 MPa and 475 MPa for 4300 s, 5800 s and 6800 s respectively.
- the maximum stresses have been shown to increase from 400 MPa for design start-up (for t = 4500s) to 558 MPa for accelerated start-up (for t = 7200s).
- for the analyzed accelerated start-up the maximum stresses did not reach the yield point of steel ST12t (Yield point Re >700 MPa), which is an important conclusion of the analysis.
- the value of temperature gradient increases twice for 2h start-up in comparison with 3h start-up
- in spite of the higher value of the stress at the accelerated start-up, it does not influence the safety of the valve operation,
- additional fatigue analyses should be carried out in order to estimate the influence of frequent changes of thermal load on valve construction.

Our attention turns especially to valves that is connected with the re-SOC technology [6]which needs a fresh-steam with high thermodynamical parameters. This technology needs large-scale steam storage that is envisioned as a key requirement in being able to both increase the flexibility of and modernize the electric gird in Poland. Electrical energy storage, actually is expected to play a crucial role in the near future (up to 2030 year) – the accelerated start-ups and shout-down are fundaments of technologies that based on the intermittent renewable sources as wind and solar [47].

Author statement

Mateusz Bryk: Conceptualization, Methodology, Software Mateusz Bryk.: Data curation, Writing- Original draft preparation. Mariusz Banaszkiewicz: Visualization, Investigation. Waldemar Duda: Supervision.: Paweł Ziółkowski: Software, Validation.: Mateusz Bryk, Tomasz Kowalczyk: Writing- Reviewing and Editing, Mateusz Bryk, Tomasz Kowalczyk, Paweł Ziółkowski: Revision of the paper.

Declaration of competing interest

The authors declare that they have no known competing financial interests or personal relationships that could have appeared to influence the work reported in this paper.

Data availability

Data will be made available on request.

References

[1] M. Banaszkiewicz, On-line monitoring and control of thermal stresses in steam turbine rotors, Appl. Therm. Eng. (2016), https://doi.org/10.1016/j.applthermaleng.2015.10.131.
[2] M. Banaszkiewicz, Online determination of transient thermal stresses in critical steam turbine components using a two-step algorithm, J. Therm. Stresses (2017), https://doi.org/10.1080/01495739.2016.1249988.
[3] A. Jalali, A. Amiri Delouei, Failure analysis in a steam turbine stop valve of a thermal power plant, Eng. Fail. Anal. (2019), https://doi.org/10.1016/j.engfailanal.2019.07.057.
[4] M. Bryk, Thermal-FSI analysis of rapid start-up of key components of thermal energy cycles in terms of cooperation with rSOC installation, in: 8th Wdzydzeanum Work. Fluid-Solid Interact., Wdzydze Kiszewskie, 2020.
[5] J. Kupecki, K. Motylinski, S. Jagielski, M. Wierzbicki, J. Brouwer, Y. Naumovich, M. Skrzypkiewicz, Energy analysis of a 10 kW-class power-to-gas system based on a solid oxide electrolyzer (SOE), Energy Convers. Manag. (2019), https://doi.org/10.1016/j.enconman.2019.111934.
[6] J. Badur, M. Lemański, T. Kowalczyk, P. Ziółkowski, S. Kornet, Zero-dimensional robust model of an SOFC with internal reforming for hybrid energy cycles, Energy (2018), https://doi.org/10.1016/j.energy.2018.05.203.
[7] R. Hyrzyński, M. Karcz, M. Lemański, K. Lewandowski, S. Nojek, Complementarity of wind and photovoltaic power generation in conditions similar to Poland, Acta Energ 17 (2013) 14–21, https://doi.org/10.12736/issn.2300-3022.2013402.
[8] P. Madejski, D. Taler, J. Taler, Modeling of Transient Operation of Steam Superheater in CFB Boiler, Energy, 2019, https://doi.org/10.1016/j.energy.2019.06.093.
[9] P. Madejski, P. Żymełka, Calculation methods of steam boiler operation factors under varying operating conditions with the use of computational thermodynamic modeling, Energy (2020), https://doi.org/10.1016/j.energy.2020.117221.
[10] R. Hyrzyński, P. Ziółkowski, S. Gotzman, B. Kraszewski, J. Badur, Thermodynamic analysis of the compressed air energy storage system coupled with the underground thermal energy storage, in: E3S Web Conf., 2019, https://doi.org/10.1051/e3sconf/201913701023.
[11] T. Kowalczyk, J. Badur, P. Ziółkowski, S. Kornet, K. Banaś, P. Ziółkowski, The problem of thermal plant flexibility under the conditions of dynamic RES development, Acta Energ 31 (2017) 116–126, https://doi.org/10.12736/issn.2300-3022.2017209.
[12] T. Kowalczyk, J. Badur, M. Bryk, Energy and exergy analysis of hydrogen production combined with electric energy generation in a nuclear cogeneration cycle, Energy Convers. Manag. 198 (2019), https://doi.org/10.1016/j.enconman.2019.111805.
[13] C. Ho, C. Siao, T. Yang, B. Chen, S. Rashidi, W. Yan, An investigation on the thermal energy storage in an enclosure packed with micro-encapsulated phase change material, Case Stud. Therm. Eng. 25 (2021), https://doi.org/10.1016/j.csite.2021.100987.
[14] M. Banaszkiewicz, Numerical investigations of crack initiation in impulse steam turbine rotors subject to thermo-mechanical fatigue, Appl. Therm. Eng. (2018), https://doi.org/10.1016/j.applthermaleng.2018.04.099.
[15] T. Kowalczyk, W. Stanek, T. Simla, Thermo-ecological evaluation of polygeneration nuclear energy cycle for electricity and hydrogen production cooperating with wind power plant, in: Proc. ECOS, 2019. Wroclaw.
[16] P. Ziółkowski, J. Badur, P.J. Ziółkowski, An energetic analysis of a gas turbine with regenerative heating using turbine extraction at intermediate pressure - brayton cycle advanced according to Szewalski's idea, Energy (2019), https://doi.org/10.1016/j.energy.2019.06.160.
[17] J. Badur, M. Bryk, Thermal-FSI modeling of the steam turbine accelerated start-up by means of cooling steam injection control, J. Power Technol. 100 (2019) 115–119.
[18] J. Badur, M. Bryk, Accelerated start-up of the steam turbine by means of controlled cooling steam injection, Energy 173 (2019), https://doi.org/10.1016/j.energy.2019.02.088.
[19] J. Badur, M. Bryk, Accelerated start-up of the steam turbine by means of controlled cooling steam injection, Energy (2019), https://doi.org/10.1016/j.energy.2019.02.088.
[20] K. Wieghardt, Siemens Steam Turbine Design for AD700 Power Plants, 2015.
[21] D. Arrell, Next generation engineered materials for ultra supercritical steam turbines, U.S Department of Energy, 2006, pp. 1–87.
[22] B. Kraszewski, A study of thermal effort during half-hour start-up and shutdown of a 400 MW steam power plant spherical Y-pipe, Case Stud. Therm. Eng. (2020), https://doi.org/10.1016/j.csite.2020.100728.
[23] A. Rusin, Numerical simulation of turbine valve creep, Arch. Appl. Mech. (1992), https://doi.org/10.1007/BF00804599.
[24] W.M. Payten, T. Wei, K.U. Snowden, P. Bendeich, M. Law, D. Charman, Crack initiation and crack growth assessment of a high pressure steam chest, Int. J. Pres. Ves. Pip. (2011), https://doi.org/10.1016/j.ijpvp.2010.11.003.
[25] Z. Chen, G. Li, H. Zhang, C. Chen, Fatigue life prediction of regulating valves on the intermediate-pressure section of a 400 MW steam turbine, Eng. Fail. Anal. (2009), https://doi.org/10.1016/j.engfailanal.2008.09.033.
[26] F. Li, B. Quay, P. Wang, D.A. Santavicca, W. Wang, S. Xu, Y. Liu, Transient thermal behaviors of a scaled turbine valve: conjugate heat transfer simulation and experimental measurement, Int. J. Heat Mass Tran. (2019), https://doi.org/10.1016/j.ijheatmasstransfer.2019.06.053.
[27] B. Cui, Z. Lin, Z. Zhu, H. Wang, G. Ma, Influence of opening and closing process of ball valve on external performance and internal flow characteristics, Exp. Therm. Fluid Sci. (2017), https://doi.org/10.1016/j.expthermflusci.2016.08.022.

[28] M.J. Chern, C.C. Wang, C.H. Ma, Performance test and flow visualization of ball valve, Exp. Therm. Fluid Sci. (2007), https://doi.org/10.1016/j.expthermflusci.2006.04.019.
[29] J. Zang, H. Yao, F. Zhang, Z. Liu, J. Meng, J. Zhu, Z. Wang, J. Qian, Dynamic characteristics analysis of pilot valves with different inlet diameters installed on the main steam valve set, SSRN Electron. J. (2022), https://doi.org/10.2139/ssrn.4017113.
[30] L. Cao, S. Liu, P. Hu, H. Si, The influence of governing valve opening on the erosion characteristics of solid particle in steam turbine, Eng. Fail. Anal. (2020), https://doi.org/10.1016/j.engfailanal.2020.104929.
[31] Z. L, H. Jia-Rong, J. Wen-Jie, R. Qiang, L. Ping, W. Jun-Mei, Z. H, Structural operability and integrity analysis of the pressure relief valve under severe accident, Case Stud. Therm. Eng. 37 (2022), https://doi.org/10.1016/j.csite.2022.102301.
[32] J. yuan Qian, L. Wei, M. Zhang, F. qiang Chen, L. long Chen, W. kang Jiang, Z. jiang Jin, Flow rate analysis of compressible superheated steam through pressure reducing valves, Energy (2017), https://doi.org/10.1016/j.energy.2017.06.170.
[33] P. Wang, H. Ma, B. Quay, D.A. Santavicca, Y. Liu, Computational fluid dynamics of steam flow in a turbine control valve with a bell-shaped spindle, Appl. Therm. Eng. (2018), https://doi.org/10.1016/j.applthermaleng.2017.10.104.
[34] F.K. Lu, D.R. Wilson, J. Matsumoto, Rapid valve opening technique for supersonic blowdown tunnel, Exp. Therm. Fluid Sci. (2009), https://doi.org/10.1016/j.expthermflusci.2008.11.009.
[35] A.A. Kendoush, Z.A. Sarkis, H.B.M. Al-Muhammedawi, Thermohydraulic effects of safety relief valves, Exp. Therm. Fluid Sci. (1999), https://doi.org/10.1016/S0894-1777(99)00013-8.
[36] Z. Orłoś, M. Augustyn, S. Dobrociński, P. Leitner, K. Tomaszewski, Experimental Studies of Temperature Fields, Deformation and Stress State under Stationary and Non-stationary Heat Loads, Theoretical calculations of thermal stress, Warsaw, 1980.
[37] P.J. Ziółkowski, T. Ochrymiuk, V.A. Eremeyev, Adaptation of the arbitrary Lagrange-Euler approach to fluid-solid interaction on an example of high velocity flow over thin platelet, Continuum Mech. Therm. (2021), https://doi.org/10.1007/s00161-019-00850-7.
[38] W. Dudda, B. Kraszewski, A theoretical validation of Burzyński hypothesis for a stress-strain analysis of heat-resistant steel, Case Stud. Therm. Eng. (2021), https://doi.org/10.1016/j.csite.2020.100806.
[39] M.T. Huber, Specific work of strain as a measure of material effort, Arch. Mech. 56 (2004) 173–190.
[40] W. Dudda, M. Banaszkiewicz, P. Ziółkowski, Validation of a Burzyński plasticity model with hardening - a case of St12T, AIP Conf. Proc. 2077 (2019).
[41] W. Dudda, Influence of high temperatures on the mechanical characteristics of 26H2MF and ST12T STEELS, Mater. Sci. (2019), https://doi.org/10.1007/s11003-019-00322-y.
[42] W. Dudda, Mechanical characteristics of 26H2MF and St12T steels under compression at elevated temperatures, Strength Mater. (2020), https://doi.org/10.1007/s11223-020-00181-y.
[43] J. Badur, P. Ziółkowski, S. Kornet, T. Kowalczyk, K. Banaś, M. Bryk, P.J. Ziółkowski, M. Stajnke, Enhanced energy conversion as a result of fluid-solid interaction in micro- and nanoscale, J. Theor. Appl. Mech. (2018), https://doi.org/10.15632/jtam-pl.56.1.329.
[44] J. Badur, M. Bryk, P. Ziolkowski, D. Slawinski, P. Ziolkowski, S. Kornet, M. Stajnke, On a comparison of Huber-Mises-Hencky with Burzynski-Pecherski equivalent stresses for glass body during nonstationary thermal load, in: AIP Conf. Proc., 2017, https://doi.org/10.1063/1.4977676.
[45] P. Duda, R. Dwornicka, Optimization of heating and cooling operations of steam gate valve, Struct. Multidiscip. Optim. (2010), https://doi.org/10.1007/s00158-009-0370-8.
[46] P. Duda, D. Rzasa, Numerical method for determining the allowable medium temperature during the heating operation of a thick-walled boiler element in a supercritical steam power plant, Int. J. Energy Res. (2012), https://doi.org/10.1002/er.1825.
[47] T. Kowalczyk, J. Badur, P. Ziółkowski, S. Kornet, K. Banaś, P.J. Ziółkowski, M. Stajnke, M. Bryk, The problem of thermal unit elasticity under the conditions of dynamic RES development, Acta Energ 31 (2017) 116–126, https://doi.org/10.12736/issn.2300-3022.2017209.